Reaction-diffusion based autonomous control of wireless sensor networks

Katsuya Hyodo and Naoki Wakamiya*

Graduate School of Information Science and Technology,
Osaka University,
Osaka, Japan
Email: k-hyodo@ist.osaka-u.ac.jp Email: wakamiya@ist.osaka-u.ac.jp
*Corresponding author

Etsushi Nakaguchi

College of Liberal Arts and Sciences,
Tokyo Medical and Dental University,
2-8-30 Kohnodai, Ichikawa,
Chiba 272-0827, Japan
Email: nakaguti.las@tmd.ac.jp

Masayuki Murata

Graduate School of Information Science and Technology,
Osaka University,
Osaka, Japan
Email: murata@ist.osaka-u.ac.jp

Yuki Kubo and Kentaro Yanagihara

Corporate Research & Development Center,
Oki Electric Industry Co. Ltd.,
2-5-7 Honmachi, Chuo-ku,
Osaka, Japan
Email: kubo635@oki.com Email: yanagihara726@oki.com

Abstract: Taking into account requirements of sensor networks, we need fully-distributed and self-organising control mechanisms which are scalable to the size of a network, robust to failures of sensor nodes, and adaptive to different and dynamically changing topology and changes in wireless communication environment. To accomplish this goal, our research group focuses on behaviour of biological systems, which inherently are scalable, adaptive and robust. In this paper, we first verify the practicality of control mechanisms adopting a reaction-diffusion equation, which explains emergence of patterns on the surface of body of fishes and mammals, and then propose two methods for faster pattern generation to save energy consumption. Prom simulation and practical experiments on a prototype, it was shown that a stable pattern could be generated in a wireless sensor network in several minutes, even when packets were lost for collisions in wireless communication.

Keywords: sensor networks; reaction-diffusion; biological system; practical experiment.

Reference to this paper should be made as follows: Hyodo, K., Wakamiya, N., Nakaguchi, E., Murata, M., Kubo, Y. and Yanagihara, K. (200X) 'Reaction-diffusion based autonomous control of wireless sensor networks', *Int. J. Sensor Networks*, Vol. X, No. Y, pp.xxx–xxx.

Biographical notes: Katsuya Hyodo received the BE degree from Kobe University, Japan, in 2006, and the ME degree from Osaka University, Japan, in 2008. He is now with Sony Corporation. His research interests include biologically inspired control mechanism for wireless sensor networks.

Naoki Wakamiya received ME and PhD degrees from Osaka University, Japan, in 1994 and 1996, respectively. He was an Assistant Professor of Graduate School of Engineering Science from April 1999 to March 2002. Since April 2002, he is an Associate Professor of Graduate School of Information Science and Technology, Osaka University. His research interests include self-organisation of overlay networks, sensor networks and mobile ad-hoc networks. He is a member of IEICE, IPSJ, ACM and IEEE.

Etsushi Nakaguchi received ME and PhD degrees from Osaka University, Japan, in 1995 and 1998, respectively. He was an Assistant Professor of Graduate School of Information Science and Technology, Osaka University, from April 2002 to March 2009. Since April 2009, he is an Associate Professor of College of Liberal Arts and Sciences, Tokyo Medical and Dental University. His research interests include pattern formation dynamics in biological systems, differential equations and numerical mathematics. He is a member of the Mathematical Society of Japan, the Japan SIAM and the Japanese Society for Mathematical Biology.

Masayuki Murata received the ME and DE degrees in Information and Computer Science from Osaka University, Japan, in 1984 and 1988, respectively. In April 1999, he became a Professor of Cybermedia Center, Osaka University, and is now with Graduate School of Information Science and Technology, Osaka University since April 2004. His research interests include computer communication networks, performance modelling and evaluation. He is an IEICE fellow and a member of IEEE, ACM, The Internet Society and IPSJ.

Yuki Kubo received the BE, the ME and the PhD degrees from University of Fukui in 2003, 2005 and 2009, respectively. In 2005, he joined Ubiquitous System Laboratory, Corporate Research and Development Center, Oki Electric Industry Co., Ltd., Osaka, Japan. His research interests include distributed autonomous systems and wireless communication networks. He is a member of the IEICE of Japan.

Kentaro Yanagihara received his BE degree in Communication Engineering and ME degree in Electric Information Systems and Energy Engineering from Osaka University, Osaka, Japan, in 2003 and 2005, respectively. In 2005, he joined Oki Electric Industry Co., Ltd., Osaka, Japan. He has been engaged in the research and development of sensor networks in the Corporate Research & Development Center.

1 Introduction

Wireless sensor network is one of the most promising and key technologies for safe, secure and comfortable society. By distributing a large number of sensor nodes and organising a network through wired/wireless communication, one can obtain detailed information about surroundings, remote region, entities and objects. Because of a large number of sensor nodes, random or unplanned deployment and dynamic topology changes due to addition, movement and removal of sensor nodes, control mechanisms for a wireless sensor network must be scalable, adaptive and robust. In addition, due to difficulty in managing a large number of nodes in a centralised fashion, mechanisms must be fully distributed and self-organising.

To establish control mechanisms with the above mentioned features, we focus on behaviour of biological systems, which inherently are scalable, adaptive and robust. For example, in Wakamiya and Murata (2005), we applied a pulse-coupled oscillator model, which explains emergence of synchronised behaviours in a group of flashing fireflies and chirping crickets, to energy-efficient data gathering. Other examples of biological mechanisms applicable to sensor networks include foraging behaviour of ants (Huang et al., 2006; Selvakennedy et al., 2006) and bees (Boonma and Suzuki, 2006), regulation of blood pressure (Dressier, 2006) and so on.

A reaction-diffusion equation is also viable as a key algorithm for autonomous control mechanisms. It was firstly proposed by Alan Turing (1952) as a mathematical model for pattern generation on the surface of body of fishes and mammals. Autonomously generated patterns on a sensor network can be used for routing, clustering, scheduling and topology control. There are some researches adopting a reaction-diffusion equation to establish an autonomous and self-organising mechanism. In smart sensor networks for a forest fire application, a stripe pattern is organised from a robot load point to a fire control point through local and mutual interactions among distributed sensor nodes and mobile robots walk along the stripe to fight a fire (Chen and Henderson, 2000). RD-MAC proposed in Durvy and Thiran (2005) is a reaction-diffusion based MAC protocol, where they noticed the similarity among a scheduling pattern of spatial TDMA and a spot pattern of leopards. A node inhibits packet emission of neighbouring nodes in its range of radio signals while encouraging nodes out of the range to send packets for better spatial use of a wireless channel. For camera sensor networks, Yoshida et al. (2005) proposed a cooperative control model for a surveillance system which consists of plural Pan-Tilt-Zoom cameras and having no central control unit is proposed. Each camera adjusts their observation area to decrease blind spots in the whole surveillance area by a control model based on a reaction-diffusion equation.

Although these work show the potential applicability of a reaction-diffusion equation to a control mechanism of a wireless sensor network, they only evaluated the proposal through simulation experiments under ideal condition. In an actual environment, sensor nodes are sparsely distributed and operate asynchronously, whereas the original reaction-diffusion equation considers the continuous space and synchronised calculation of the equation. In addition, a sensor node has the limited computational capability, integer arithmetic is preferred for high-speed operation, whereas a reaction-diffusion equation requires real number calculation. Integer arithmetic reduces the accuracy of calculation and a desired pattern could not be generated. Furthermore, faster pattern generation is preferred in a wireless sensor network, since diffusion process which involves message exchanges among sensor nodes and consumes energy. Therefore, in this paper, we conduct both of simulation and practical experiments to verify the practicality of reaction-diffusion based pattern generation in an actual

environment. In addition, to have an energy-efficient control, we propose two methods to accelerate pattern generation. We further evaluate the influence of packet loss considering a practical scenario.

The rest of the paper is organised as follows. In Section 2, we introduce a reaction-diffusion equation that our paper is based on. Next in Section 3, we describe our reaction-diffusion based control mechanism for a wireless sensor network. In Section 4, we then show and discuss results of simulation and practical experiments. Finally, we conclude the paper in Section 5.

2 Reaction-diffusion equation

A reaction-diffusion equation of two morphogens, i.e. activator and inhibitor, can be written as

$$\begin{cases} \dfrac{\partial u}{\partial t} = F(u,v) + D_u \nabla^2{}_u \\ \dfrac{\partial v}{\partial t} = G(u,v) + D_v \nabla^2{}_v \end{cases} \tag{1}$$

where u and v are the concentrations of activator and inhibitor, respectively. The first term of the right-hand side is a reaction team and the second term is a diffusion term. F and G are nonlinear functions for chemical reactions. D_u and D_v are the diffusion rate of activator and inhibitor, respectively. ∇^2 is the Laplacian operator.

In a reaction-diffusion mechanism, the following conditions must be satisfied to generate patterns; (1) The activator activates itself and the inhibitor, whereas the inhibitor restraints the activator and (2) The inhibitor diffuses faster than the activator ($D_v > D_u$). A mechanism of pattern generation can be explained as follows. In Figure 1, those hypothetical chemicals are arranged in a line on the x-axis. The y-axis corresponds to the concentrations of activator and inhibitor. Now, consider that the concentration of activator has a peak at the centre by a slight perturbation. The concentrations of activator and inhibitor are increased around the peak by self-activation. The generated inhibitor diffuses faster than the activator and restrains generation of activator at further regions. On the other hand at the peak, the concentration of activator is kept higher than that of inhibitor for different rates of diffusion. Consequently, the diversity in the concentration of activator emerges and a pattern appears. For example, when we colour a point where the concentration of activator exceeds a certain threshold with white and others with black, we can see a black-white-black pattern shown at the bottom of Figure 1.

In this paper, we use the equations below for F and G, which model pattern generation on an emperor angelfish *Pomacanthus imperator* (Kondo and Asai, 1995).

$$\begin{cases} F(u,v) = \max\{0, \min\{au - bv + c, M\}\} - du \\ G(u,v) = \max\{0, \min\{eu + f, N\}\} - gv, \end{cases} \tag{2}$$

where a and e correspond to the rate of activation and b is for that of inhibition, c and f are parameters for synthesis or increase of morphogens per unit time, d and g are for decomposition or decrease of morphogens per unit time. M and N are constants of limit. Figure 2 illustrates chemical reactions of the morphogens following the reaction-diffusion equation.

Figure 1 Pattern generation

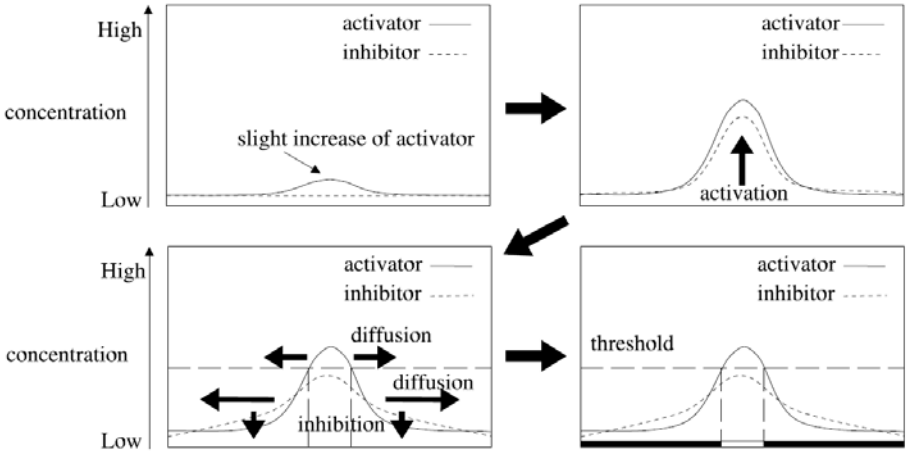

Figure 2 Dynamics of morphogens

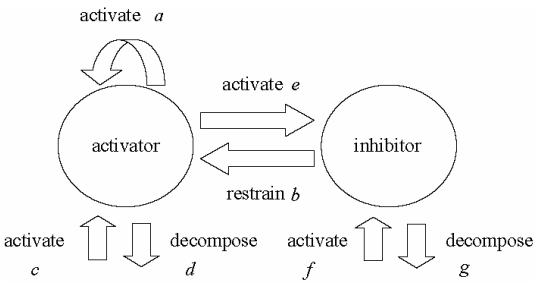

In order to generate patterns, the parameters must satisfy Turing conditions shown below.

$$a - d - g < 0, \tag{3}$$

$$eb - (a-d)g > 0, \tag{4}$$

$$D_v(a-d) - D_u g > 0, \tag{5}$$

$$\left(D_v(a-d) - D_u g\right)^2 - 4D_u D_v\left(eb - (a-d)g\right) > 0. \tag{6}$$

As far as these conditions are satisfied, the space will have the spatial heterogeneity in terms of the concentration of morphogens and a variety of patterns can be generated as illustrated in Figure 3. Derivation of the Turing conditions is described in Appendix A.

Figure 3 Example of generated patterns

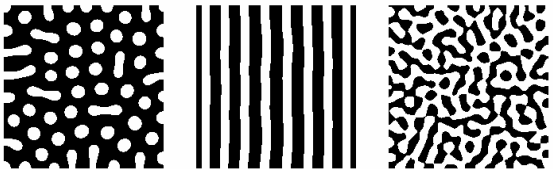

(a) spots (b) stripes (c) maze

If the initial concentrations of activator and inhibitor are both larger than zero, u and v have the upper limit $u_{\max} = r/d$ and $v_{\max} = s/g$, respectively. The lower limits are $u_{\min} = v_{\min} = 0$. By regarding $F(u, v)$ as $(a - d)u - bv + c$ and $G(u, v)$ as $eu - gv + f$, wavelength l of a generated pattern can be derived as,

$$l = 2\pi \sqrt[4]{\frac{D_u D_v}{eb - (a - d)g}}. \tag{7}$$

Derivation of the wavelength is described in Appendix B.

3 Reaction-diffusion based control mechanism

To verify the practicality of a reaction-diffusion based mechanism, we consider a simple and general mechanism described as follows.

Nodes are arranged in a grid network topology, where a node can communicate with four direct neighbours in up, down, left and right directions. Nodes at a corner have two neighbours and nodes at an edge have three neighbours. At regular intervals, a node calculates the reaction-diffusion equation by using information about morphogen concentrations of neighbours, which it has received after the previous control timing. Then, it broadcasts information about its morphogen concentrations to the neighbours. If a node did not receive concentration information from a neighbour in this interval, it uses the latest information it received instead. Nodes behave in an asynchronous manner. It means that timing of message emission and reaction-diffusion calculation are different among nodes.

Since the arrangement of nodes and exchange of information are discrete in space and time, we first discretise equation (1) as follows:

$$\begin{aligned} u_{t+1} &= u_t + \Delta t \\ &\left\{ F(u_t, v_t) + D_u \frac{\left(u_t^u + u_t^d + u_t^l + u_t^r - 4u_t\right)}{\Delta h^2} \right\} \\ v_{t+1} &= v_t + \Delta t \\ &\left\{ G(u_t, v_t) + D_u \frac{\left(v_t^u + v_t^d + v_t^l + v_t^r - 4v_t\right)}{\Delta h^2} \right\}. \end{aligned} \tag{8}$$

At the t-th control timing, a node calculates the reaction-diffusion equation to obtain its morphogen concentrations u_{t+1} and v_{t+1}, based on which a node decides its behaviour, e.g. colour, in the next control interval. A set of u_t^u, u_t^d, u_t^l and u_t^r and a set of v_t^u, v_t^d, v_t^l and v_t^r correspond to neighbouring nodes' concentrations of activator and inhibitor that a node uses for calculation at the t-th control timing, respectively. Δh and Δt correspond to the distance between nodes and the discrete step interval of time, respectively. There is the range of Δt for the equation reaches convergence,

$$0 < \Delta t < \min \left\{ \frac{2}{d + 4D_u\left(\Delta x^{-2} + \Delta y^{-2}\right)}, \frac{2}{g + 4D_v\left(\Delta x^{-2} + \Delta y^{-2}\right)} \right\}. \tag{9}$$

As far as the degree of temporal discretisation is within this range, the same pattern is generated for the same set of parameters.

Since a sensor node has the limited computational capability, integer arithmetic is preferred for high-speed operation. However, integer arithmetic introduces several problems such as truncation error, cancellation error, loss of trailing digit and overflow. When the number of significant digits is insufficient, a generated pattern becomes different from that obtained by real number computation or a pattern does not converge. In this paper, we set the number of significant digits as four. Since concentrations of activator and inhibitor range from 0 to M and N and they are set at 0.2 and 0.5, respectively, we multiply the concentrations by 10^3 to have four-significant-digit numbers. We confirmed this was sufficient from simulation experiments.

When we consider to generate a pattern under random node layout, we should further discretise $\nabla^2 X\left(X = u, v\right)$ as follows:

$$\nabla^2 X = \sum_{j \neq i} k_{i,j}\left(X_j - X_i\right) \tag{10}$$

$$k_{i,j} = \begin{cases} d_{i,j}^{-2}, & d_{i,j} \le R, \\ 0, & \text{otherwise} \end{cases} \tag{11}$$

where, X_i and X_j are the concentration of morphogens in node i and j and $d_{i,j}$ is the distance between the two nodes. R is the maximum transmission range. We confirm the pattern generation of this equation by simulation experiments. An example of a generated pattern is shown in Figure 4. In the figure, squares show nodes and the brighter colour indicates lower concentration of activator. From this Figure, we can see that the spot patterns appear in random node layout. For simple analysis, we use the grid node layout in following simulations.

Figure 4 Simulation result of random node layout (see online version for colours)

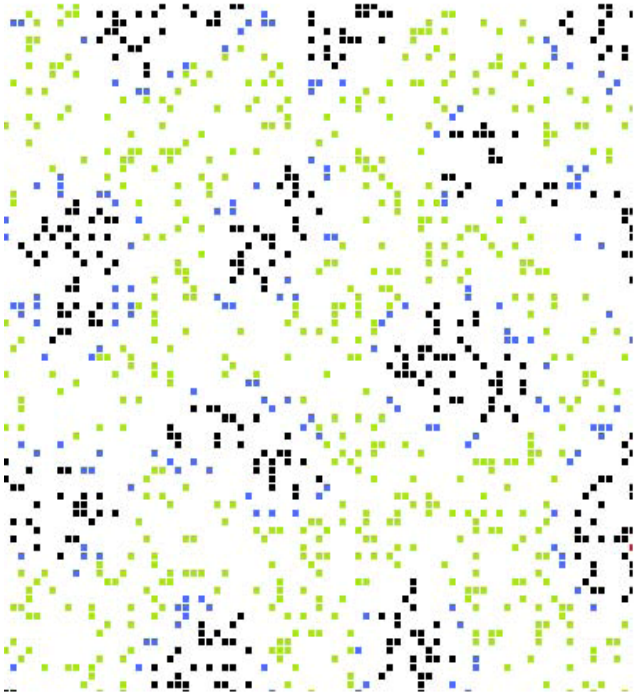

4 Simulation and practical experiments

In this section, we show results of simulation and practical experiments and discuss the practicality and applicability of the reaction-diffusion based mechanism.

4.1 Simulation experiments

First, we verify the appropriateness of our spatial discretisation of the reaction-diffusion equation. Nodes are arranged in a 100 × 100 grid network. At the beginning of a simulation run, the concentrations of activator and inhibitor of the node at (50, 50) are set at 5000 and 3000, respectively. The concentrations at the other nodes are all set at 3000. Some results of comparison among simulation and analysis are illustrated in Figure 5 for the wavelength of generated patterns. Parameters are summarised in Table 1, which satisfy the Turing conditions. The wavelength of a pattern generated by simulation is obtained by averaging the sum of widths of black and white stripes over stripes. As shown in the figures, the results match among simulation and analysis. With the finer spatial discretisation with a smaller Δh, results become closer. We also evaluated the upper limit of temporal discretisation ΔT and simulation and analysis had good matches, but results are not shown in the paper due to the space limitation.

Figure 5 Comparison of simulation and analysis: wavelength

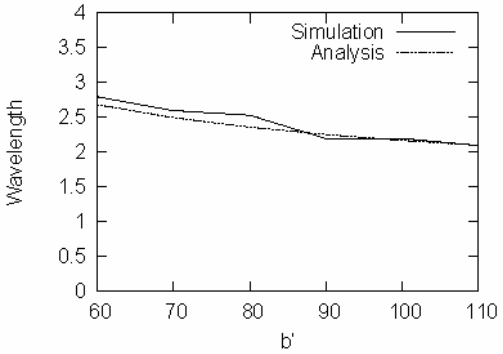

(a) $60 < b' < 110, D'_v = 50$

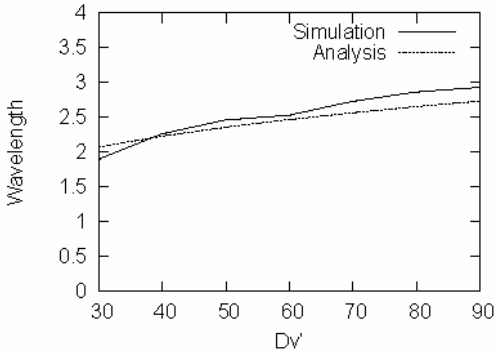

(b) $b' = 80, 30 < D'_v < 90$

Table 1 Parameters used for wavelength comparisons

Parameter	*Value*	*Parameter*	*Value*
a'	80	D'_u	2
b'	60–110	D'_v	30–90
c'	20	M'	200000
d'	30	N'	500000
e'	100	ΔT	1
f'	–150	Δh	0.2
g'	60		

Next, we evaluate the mathematical upper limit of temporal discretisation ΔT. Nodes are arranged in a 5 × 5 grid network. Parameters are summarised in Table 2. In Figure 6, comparisons among simulation and analysis are shown. We conducted simulation experiments by changing ΔT from 1 by 1 to obtain the upper limit of generating a stable pattern. We can see that the results are similar among simulation and analysis, but the limit of simulation is always larger than that of analysis. The reason for this is that non-linear clauses of equation (2) are not taken into account in derivation of equation (9).

Table 2 Parameters used for ΔT comparisons

Parameter	*Value*	*Parameter*	*Value*
a'	80	D'_u	2
b'	80	D'_v	50–200
c'	20	M'	200000
d'	20–40	N'	500000
e'	100	ΔT	1–100
f'	–150	Δh	1
g'	50–110		

Figure 6 Comparison of simulation and analysis: limit on ΔT

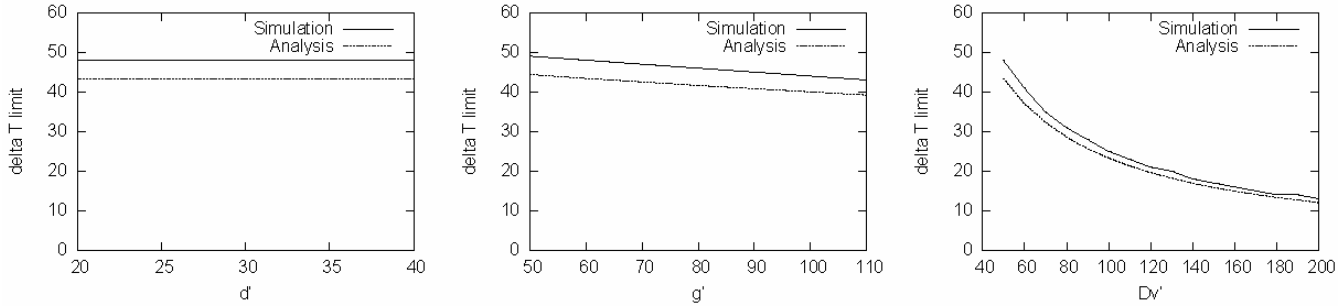

(a) $20 < d' < 40, g' = 60, D'_v = 50$ (b) $d' = 30, 50 < g' < 110, D'_v = 50$ (c) $d' = 30, g' = 60, 50 < D'_v < 200$

Figure 7 illustrates a stable pattern generated on a 5 × 5 grid network with a set of parameters in Table 3. A white square corresponds to a node with the concentration of activator higher than 3000. A black square is for a node with the concentration of activator smaller than 3000. Since we set a peak of the concentration of activator at the centre, a generated pattern forms concentric circles.

Figure 7 Generated pattern by simulation

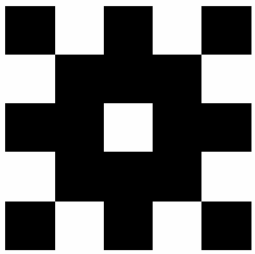

Table 3 Parameter setting

Parameter	*Value*	*Parameter*	*Value*
a'	80	D'_u	2
b'	80	D'_v	50
c'	20	M'	200000
d'	30	N'	500000
e'	100	ΔT	1
f'	–150	Δh	1
g'	60		

Pattern generation normally takes time and requires a considerable number of calculations. It further corresponds to the number of communication and the energy consumption. Therefore, we need to accelerate pattern generation for energy-efficient and adaptive controls. We propose two methods: (a) to have a larger discrete step ΔT and (b) to calculate the reaction-diffusion equation for K times at each control timing.

Figure 8 show results of changing ΔT to 1, 10 and 40 by using the method (a). The other parameters are set based on Table 3. The theoretical upper limit of ΔT is 43.5. Generated patterns are the same among all. Figure 8(a) illustrates the transition of concentration of activator at the node at the upper left corner against the number of communication and calculations. The number of communication corresponds to the number of messages that a node emits and it is equivalent to the number of control intervals. Since a node calculates the reaction-diffusion equation once per control interval, the number of communication and the number of calculations are identical for the method (a). As shown in Figure 8(a), the number of communication and calculations required for the convergence of concentration of activator can be decreased by increasing ΔT. However, the faster convergence is achieved at the sacrifice of the accuracy of calculation. Figure 8(b) shows the transition of concentration of activator against the elapsed time in reaction-diffusion calculation. The elapsed time is derived by multiplying ΔT by the number of communication or calculations. We can see that a larger ΔT leads to larger fluctuation, because the accuracy of calculation becomes lower with a larger ΔT for discretisation. However, in our simulation experiments, all ΔT within the range of equation (9) result in the same stable pattern illustrated in Figure 7.

Next, we evaluate the method (b). Figure 9 shows results of changing K as 1, 10 and 40. The other parameters are set as Table 3. Generated patterns are the same among all independently of K. In the case of the method (b), at regular control timing, a node calculates the reaction-diffusion equation for K times by using the same concentration values for neighbouring nodes, and then broadcasts the result. Therefore, the number of calculations is K times larger than the number of communication. In Figure 9(a), the transition of concentration of activator is depicted against the number of communication for different setting of K. As shown, a larger K decreases the number of communication required for convergence. Since a larger K spoils the accuracy of reaction-diffusion calculation as a larger ΔT does, the transitions of concentration of activator are similar among Figure 8(b) and Figure 9(b). K also has the limitation on the effective range to generate a pattern. When K is greater than 130, the concentration of activator does not converge and a pattern becomes unstable. In the range of $40 < K < 130$, the number of communication required to reach a stable pattern does not change. Therefore, the effective range of K is from 0 to 40. Figure 10 illustrates comparison among the methods, where $K = 1$ and $\Delta T = 10$ for the method (a) and $K = 10$ and $\Delta T = 1$ for the method (b). As shown in the Figure, those methods show quite similar behaviour.

Figure 8 Simulation result of method (a)

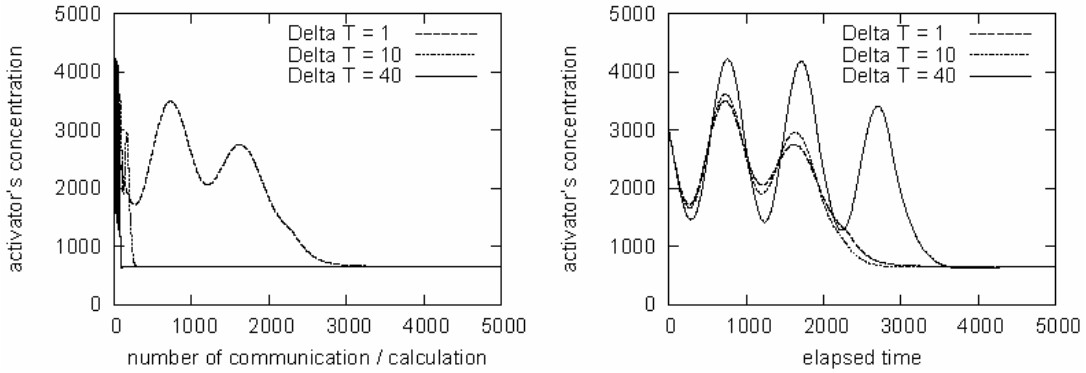

(a) Transition of concentration of activator against number of communication and calculation

(b) Transition of concentration of activator against elapsed time

Figure 9 Simulation result of method (b)

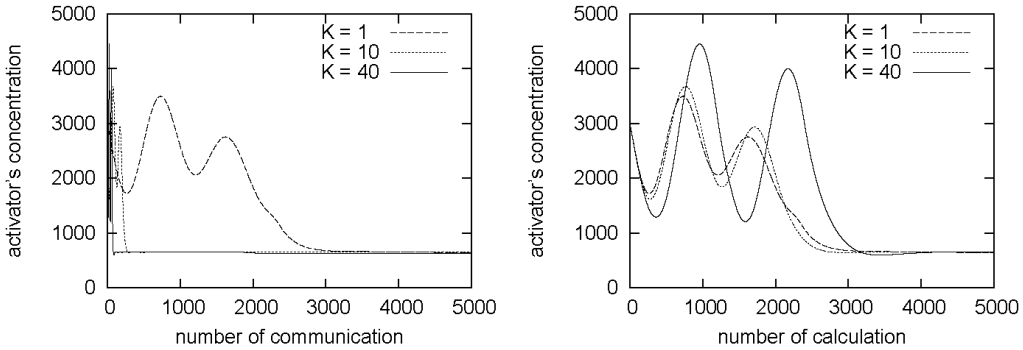

(a) Transition of concentration of activator against number of communication

(b) Transition of concentration of activator against number of calculations

Figure 10 Comparison among methods

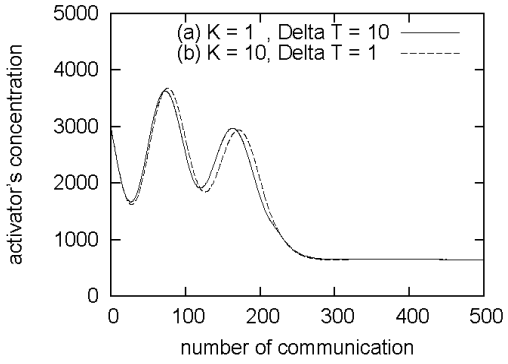

Although the proposed methods can effectively reduce the number of communication, it sacrifices the robustness against information loss. Figure 11 shows the probability of successful pattern generation against the information loss rate. We assume that the information about concentrations is lost at random at the information loss rate. The probability of successful pattern generation is defined as the ratio of simulation runs which reach the same stable pattern that is generated for the case without loss of information to all 1000 simulation runs. As shown in Figure 11, our acceleration methods can generate a stable pattern under random information loss of 4%, whereas a normal mechanism without acceleration can tolerate up to 23% random information loss. Therefore, we need an additional mechanism, such as retransmission, to generate patterns under unstable and unreliable radio conditions.

Figure 11 Influence of information loss

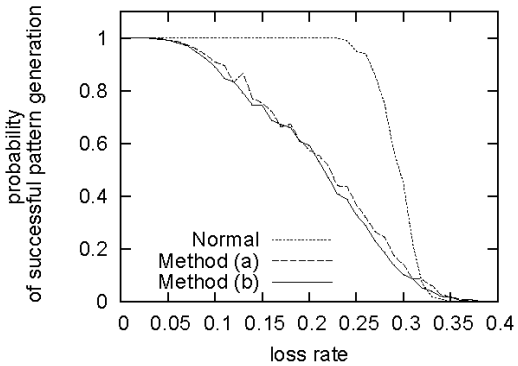

4.2 Practical experiments

We implement the reaction-diffusion based mechanism using off-the-shelf nodes of OKI Electric Industry (Figure 12). We added a board with large LEDs for better visualisation of pattern generation. 25 nodes are arranged in a 5 × 5 grid

network. All nodes use the same reaction-diffusion equation of the same parameter setting in Table 3 and adopt the method (a) with $\Delta T = 10$. A node uses IEEE 802.15.4 non-beacon mode MAC protocol. 32 bit signed integer is used for calculation. All nodes are in the range of radio signals of each other. Therefore, to restrict nodes to communicate among direct neighbours, we introduce a MAC address-based filter. A node maintains a list of MAC addresses of neighbouring nodes to communicate with, and it only receives packets originated from nodes in the list. A packet broadcast by a node is of 32 bytes including a header, the concentrations of activator and inhibitor, the total number of calculations it has conducted, and the total number of packets it has not received. The last two are for logging and debugging purpose.

Figure 12 Prototype (see online version for colours)

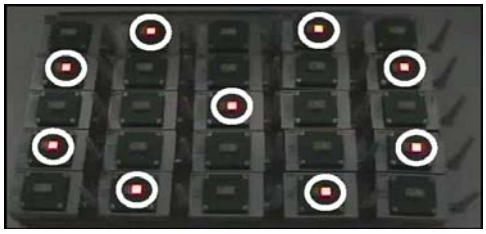

We determine the control interval to keep the average loss rate less than 4%. If the control interval is too short, nodes behave in synchrony and the loss rate becomes high for collision and congestion. We conducted preliminary experiments by changing the control interval and found that the control interval must be larger than about 700 msec to keep the loss rate below 4%. Therefore, we empirically set the control interval as 1400 msec taking into account dynamic changes in wireless communication environment.

In Figure 12, nodes with a LED on are indicated by circles. A node turns on its LED when the concentration of activator is higher than 3000. In comparison to Figure 7, it is verified that the prototype can generate the same pattern as in simulation. Figure 13 shows the detailed comparison. There is no loss of information in simulation, whereas the average packet loss rate is about 3% on the prototype. Nevertheless, transitions of concentration of activator are almost the same among the prototype and simulation. Therefore, we can conclude that the reaction-diffusion based pattern generation works on an actual wireless sensor network and the number of communication, i.e. the amount of energy consumption, can be reduced by our acceleration methods with appropriately chosen parameters.

Figure 13 Comparison among simulation and implementation

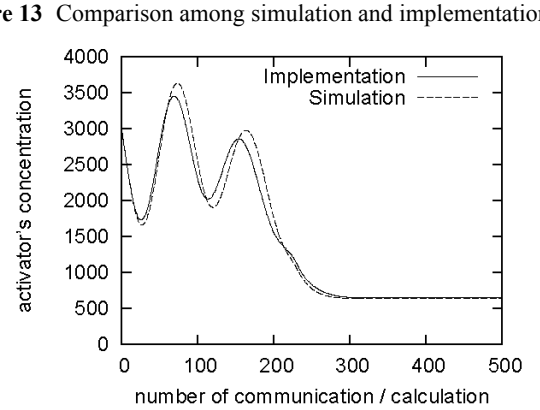

5 Conclusion

In this paper, we verified the practicality of reaction-diffusion based control mechanisms for wireless sensor networks by simulation and practical experiments. Whereas sensor nodes are placed in a discretised manner, they exchange concentration information and calculate equations intermittently and asynchronously, and there is loss of information due to packet losses, a wireless sensor network could successfully generate an intended pattern based on the reaction-diffusion model.

We also proposed and evaluated two methods to accelerate pattern generation for energy-efficiency. As far as the temporal discretisation ΔT and the number of calculations K are kept within a certain limit, we can accelerate the speed of pattern generation in the two orders of magnitude, which further leads to considerable saving of energy and wireless bandwidth.

Our proposed discretisation and acceleration methods are useful to make other reaction-diffusion based mechanisms realistic and practical. Based on the results, We also proposed a new self-organising and autonomous clustering mechanism based on a reaction-diffusion model, where we regarded spots in a reaction-diffusion pattern as clusters centred at a cluster head (Wakamiya et al,. 2008).

Acknowledgements

This work was partly supported by 'Special Coordination Funds for Promoting Science and Technology: *Yuragi Project*', Grant-in-Aid for Scientific Research on Priority Areas 18049050 and a Grant-in-Aid for Scientific Research (A) (2) 16200003 of the Ministry of Education, Culture, Sports, Science and Technology in Japan.

References

Boonma, P. and Suzuki, J. (2006) 'Biologically-inspired data aggregation for multi-modal wireless sensor networks', *Proceedings of the 31st IEEE Conference on Local Computer Networks (LCN 2006)*.

Chen, Y. and Henderson, T.C. (2000) 'S-nets: smart sensor networks', *Proceedings of International Symposium on Experimental Robotics (ISER 2000)*, pp.85–94.

Dressier, F. (2006) 'Bio-inspired promoters and inhibitors for self-organized network security facilities', *Proceedings of the 1st IEEE/ACM International Conference on Bio-Inspired Models of Network (BIONETICS 2006)*, pp.1–7.

Durvy, M. and Thiran, P. (2005) 'Reaction-diffusion based transmission patterns for ad hoc networks', *Proceedings of the IEEE Conference on Computer Communications (INFOCOM 2005)*, Vol. 3, pp. 2195–2205.

Huang, R., Zhu, J., Yu, X. and Xu, G. (2006) 'The ant-based algorithm for the optimal many-to-one routing in sensor networks', *Proceedings of International Conference on Communications, Circuits and Systems (ICCCAS 2006)*, Vol. 3, pp.1532–1536.

Kondo, S. and Asai, R. (1995) 'A reaction-diffusion wave on the kin of the marine angelfish Pomacanthus', *Nature*, Vol. 376, pp.765–768.

Selvakennedy, S., Sinnappann, S. and Shang, Y. (2006) 'T-ANT: a nature-inspired data gathering protocol for wireless sensor networks', *Journal of Communication*, Vol. 1, No. 2, pp.22–29.

Turing, A.M. (1952) 'The chemical basis of morphogenesis', *Royal Society of London Philosophical Transactions Series B*, Vol. 237, pp.37–72.

Wakamiya, N., Hyodo, K. and Murata, M. (2008) Reaction-diffusion based topology self-organization for periodic data gathering in wireless sensor networks', *Proceedings of 2nd IEEE International Conference on Self-Adaptive and Self-Organizing Systems (SASO 2008)*, pp.351–360.

Wakamiya, N. and Murata, M. (2005) 'Synchronization-based data gathering scheme for sensor networks', *IE-ICE Transaction on Communications, Special Section on Ubiquitous Networks*, E88-B, pp.873–881.

Yoshida, A., Aoki, K. and Araki, S. (2005) 'Cooperative control based on reaction-diffusion equation for surveillance system', *Proceedings of 9th International Conference on Knowledge-Based Intelligent Information and Engineering Systems (KES 2002),* pp.533–539.

Appendix A: Turing conditions

Turing conditions must be satisfied for a reaction-diffusion equation to have Turing instability. When the spatially uniform steady state which keeps stable against a small spatially uniform perturbation becomes unstable against a small spatially non-uniform perturbation, the system is considered to have Turing instability.

Equations (1) and (2) have only one uniform steady state (u_e, v_e) shown as follows.

$$u_e = \frac{bf + gc}{eb - (a-d)g},\ v_e = \frac{(a-d)f + ec}{eb - (a-d)g} \tag{A1}$$

Linear partial differential equations can be derived by linearising equations (1) and (2) considering small perturbation $\xi = u - u_e$ and $\eta = v - v_e$ from the uniform steady state as,

$$\begin{cases} \dfrac{\partial \xi}{\partial t} = (a-d)\xi - b\eta + D_u \Delta \xi \\ \dfrac{\partial \eta}{\partial t} = e\xi - g\eta + D_v \Delta \eta \end{cases} \tag{A2}$$

Since equation (A2) is linear, the solution (ξ, η) is given by the sum of eigenmode (ξ_μ, η_μ) for eigenvalue μ of an operator Δ. Behaviour of eigenmode (ξ_μ, η_μ) follows the following differential equations.

$$\begin{cases} \dfrac{\partial \xi_\mu}{\partial t} = (a-d)\xi_\mu - b\eta_\mu + D_u \mu \Delta \xi_\mu \\ \dfrac{\partial \eta_\mu}{\partial t} = e\xi_\mu - g\eta_\mu + D_v \mu \Delta \eta_\mu \end{cases} \tag{A3}$$

It can be evaluated by the root of the following quadratic polynomial.

$$p_\mu(\lambda) = \big(\lambda + D_u\mu - (a-d)\big)(\lambda + D_u\mu + g) + eb \tag{A4}$$

If $p_\mu(\lambda)$ has a root with one or more positive real parts, eigenmode (ξ_μ, η_μ) diverges. When conditions of equations (A5) and (A6) below are satisfied, both roots of $P_o(\lambda)$ have a negative real part.

$$a - d - g < 0 \tag{A5}$$

$$eb - (a-d)g > 0 \tag{A6}$$

Therefore, (ξ_μ, η_μ) converge to (0, 0) as time passes. In other words, (u_e, v_e) is stable against a spatially uniform perturbation.

In order for the uniform steady state (u_e, v_e) to have Turing instability, it is necessary that at least one of roots of $P_\mu(\lambda)$ to have a positive real part for a positive eigenvalue μ. From equations (A5) and (A6), if $\mu > 0$, $(D_u + D_v)\mu - (a-d) + g > 0$ holds. Therefore, the following equation should be satisfied for a positive real number μ.

$$h(\mu) = \big(D_u\mu - (a-d)\big)(D_v\mu + g) + eb < 0 \tag{A7}$$

Since $D_uD_v > 0$ and $eb - (a-d)g > 0$, both roots of $h(\mu)$ must have a positive real number. Consequently, the following conditions must be satisfied.

$$Dv(a-d) - Dug > 0 \tag{A8}$$

$$\big(D_v(a-d) - D_u g)^2 - 4D_uD_v(eb - (a-d)g\big) > 0 \tag{A9}$$

Equations (A5), (A6), (A8) and (A9) are Turing conditions for the reaction-diffusion equations (1) and (2).

Appendix B: Wavelength

A reaction-diffusion equation which satisfies Turing conditions has Turing instability. Turing instability cause two divergences, Hopf divergence and Turing divergence. Hopf divergence causes the steady state to periodically change, whereas Turing divergence does not. Here, we consider Turing divergence. When a root of $p_\mu(\lambda)$ changes from a negative number to a positive number and the other root is a negative number, Turing divergence happens. In other words, discriminant of $h(\mu)$,

$$\Delta_h = \big(D_v(a-d) - D_u g\big)^2 - 4D_uD_v\big(eb - (a-d)g\big), \tag{B1}$$

changes from positive to negative, $\mu = \mu_C$ that makes $h(\mu)$ to 0 when $\Delta_h = 0$ is shown below.

$$\mu_c = \frac{D_v(a-d) - D_u g}{2D_uD_v} \tag{B2}$$

The corresponding mode becomes unstable and generates a steady state pattern. $D_v(a-d) - D_u g = 2\sqrt{D_uD_v\big(eb - (a-d)g\big)}$, because $\Delta_h = 0$. Then, the following holds,

$$\mu_c = \sqrt{\frac{eb - (a-d)g}{D_uD_v}}. \tag{B3}$$

Finally, the wavelength of eigenmode l is given as,

$$l = \frac{2\pi}{\sqrt{\mu}} = 2\pi\sqrt[4]{\frac{D_uD_v}{eb - (a-d)g}}. \tag{B4}$$